Joint Centre for Mesoscale Meteorology, Reading, UK

Longwave Radiative Forcing of a Simulated Tropical Sqall Line

I. Dharssi

Internal Report No. 34

July 1994

Met Office Joint Centre for Mesoscale Meteorology Department of Meteorology
University of Reading PO Box 243 Reading RG6 6BB United Kingdom
Tel: +44 (0)118 931 8425 Fax: +44 (0)118 931 8791
www.metoffice.com

Longwave Radiative Forcing Of A Simulated Tropical Squall Line

by
Imtiaz Dharssi

July 1994

Abstract

This article describes a tropical squall line simulation and compares model results with observations and other simulations. Preliminary results are described and a sensitivity study is performed which shows that longwave radiative heating increases total surface rainfall and the size of the anvil.

1 Introduction

Recent work has shown that radiative heating and cooling can significantly modulate the behaviour of convective systems. Using a two-dimensional model to study convection observed during the winter monsoon experiment over the south China sea, Dudhia (1989) finds that radiation significantly enhances convection. This effect is attributed primarily to large scale longwave radiative cooling which counters warming due to the convection. Although longwave radiative cooling extends to the surface, enhanced surface fluxes means that θ_e reduces more slowly in the boundary layer than in the midtroposphere. Therefore, this tends to destabilise the domain and increases convective activity. Gray and Jacobson (1977) propose that differential radiative cooling between clear and cloudy regions generates a secondary circulation which enhances cloud activity. Within the cloud interior there is very little longwave radiative cooling. Thus the clear air surrounding the cloud experiences significantly greater radiative cooling than the cloudy air. This leads to subsidence in the clear air which induces convergence into the cloud region. Webster and Stephens (1980) suggest that convective overturning will occur in stratiform clouds due to radiative cloud base warming and cloud top cooling. Observations also indicate the importance of radiation on convection; Gray and Jacobson (1977) find evidence of a single diurnal cycle with an early morning maximum of heavy precipitation for deep tropical maritime convection.

This article describes a simulation of a tropical squall line and the results of experiments to determine the system's sensitivity to longwave radiative heating and cooling. Observations from EMEX9 (Equatorial Mesoscale Experiment; aircraft mission 9) are used to initialize the model. The EMEX9 system developed over the Arafura sea between Australia and New Guinea and is chosen for the simulation because the synoptic conditions and observations of this system have already been described by Webster and Houze (1991). In addition this system has been simulated by Tao et al (1993) and Wong et al (1993) allowing for some comparison of results.

Section 2 briefly describes the cloud model. Section 3 describes the longwave radiation scheme used within the cloud model. Section 4 describes the simulation including initial conditions. Section 5 describes the results of sensitivity experiments. Section 6 discusses the results and offers some conclusions.

2 Model

The model used for this study is the two-dimensional version of the Meteorological Office cartesian Large Eddy Simulation model (described by Derbyshire and Kershaw, 1993). This model is formulated using the deep anelastic quasi-Boussinesq equation set which is a generalization of the incompressible Boussinesq equation set. This model is non-hydrostatic and excludes sound waves. The cloud microphysics scheme includes a Kessler type parametrization for liquid water and a three category ice-phase scheme (cloud ice, snow, graupel). The conversion rates between categories are based on the bulk-water parametrization of Lin, Farley and Orville (1983). The size spectra for each precipitation type is assumed to be an inverse exponential. Details of this scheme are given by Swann (1994).

The model uses a stretched vertical grid with 31 levels and the model top at $20\,km$. Height increment vary from about $400\,m$ near the surface to $1500\,m$ at the top. The model has 1000 grid points in the horizontal with a constant resolution of $750\,m$. Periodic boundary conditions are used for the lateral boundaries.

3 Longwave radiation parametrization

The longwave parametrization scheme implemented within the cloud model is based on the scheme used by the Meteorological Office Unified Model as described by Ingrams (1993) and Slingo and Wilderspin (1986). This parametrization scheme solves the radiative transfer problem for each model column in terms of a vertically upward and a vertically downward longwave flux. Such an approach is only strictly valid for a plane parallel atmosphere. For gaseous absorption, variations in the vertical are much larger than variation in the horizontal and thus the 'plane parallel' approximation will give good results. However clouds can show significant horizontal variation and it is not clear how valid the 'plane-parallel' approximation remains in this case. Even stratiform clouds such as stratocumulus are not truly horizontally homogeneous. For example, the tops of stratocumulus clouds are undulating and this is likely to effect their radiative properties. Unfortunately radiative schemes which include the horizontally finite extent of clouds are computationally very expensive and it remains impossible to include such a scheme within a cloud model.

The longwave radiation scheme includes absorption by water vapour, carbon dioxide, ozone, cloud water and cloud ice. Only the effects of absorption and emission are in-

cluded and scattering is ignored. However, it is generally believed that scattering is not important for longwave radiation. For gaseous absorption a lookup table is used to obtain transmissivities from absorber pathlength. This pathlength is scaled to include the effects of collision and doppler broadening of the absorption lines.

A model grid box is assumed to either be completely filled by cloud or to contain no cloud (partial cloud cover within a grid box is not allowed). This approximation is reasonable given the relatively high resolution of the model. For cloud water the emissivity is calculated from an equation derived by Stephens (1984) using results from Mie theory. Only the cloud water path (cloud water content $\times$ layer width) is required. Thus the emissivity is given by

$$\epsilon = 1 - \exp\left(-\kappa\, CWP\right), \tag{1}$$

where CWP is the cloud water path and $\kappa = 130\, m^2 kg^{-1}$.

The longwave scheme treats absorption by cloud ice in a similar way to cloud water. The absorption properties of ice are assumed to depend only on the ice water content and the difference in the absorption properties of ice and water is accounted for by a scaling constant. Thus $\kappa_{Ice} = 65\, m^2 kg^{-1}$. However, both experiment and theory show that this is an over-simplification and that the effective radius of the ice particles as well as the ice water content is important. Francis et al (1994) measured values of κ_{Ice} ranging from $3\, m^2 kg^{-1}$ to $144\, m^2 kg^{-1}$. The reason for this large variation is that κ_{Ice} has an inverse dependence on the ice crystal effective radius, as predicted by simple theory. The value of κ_{Ice} used in the Unified model corresponds to an ice crystal effective radius of about $20\, \mu m$. The ice microphysics scheme can be used to derive an ice crystal effective radius but it is not clear how reliable such an estimate would be. Thus for simplicity κ_{Ice} is kept fixed. The longwave scheme ignores the effect of rain, snow and graupel.

4 Model Simulation

This section describes some of the features of the modelled squall line and compares these with observations and previous simulation studies by Tao et al (1993) and Wong et al (1993). The simulation including cooling/heating by longwave radiation is described although the results from the simulation with no longwave radiation are qualitatively similar.

4.1 Initial Conditions

Both Tao et al (1993) and Wong et al (1993) have simulated the EMEX9 system. However, their initial conditions appear quite different. Tao et al (1993) used a combination of observations from EMEX9. Below $400\,mb$, measurements from the NCAR Electra aircraft ahead of the system were used. While above $400\,mb$ data interpolated from radiosonde profiles and objective analyses were used. Wong et al (1993) used primarily the radiosonde profile for Darwin, Australia. Probably of most importance are the differences in the wind profile used. Both wind profiles have a low level jet with maximum speed of approximately $15\,ms^{-1}$, but for Tao et al (1993) the jet is at about $850\,mb$ while Wong et al (1993) have the jet at about $550\,mb$. Above $700\,mb$ the wind profile used by Tao et al (1993) has very little shear and the wind is close to $7.5\,ms^{-1}$. In contrast the wind profile used by Wong et al (1993) has strong shear at all levels and the wind has a minimum (large negative) value of $-18\,ms^{-1}$ at $100\,mb$.

Tao et al (1993) impose a large scale forced ascent over the entire model domain. One effect of this is that conditions for the squall line are always favourable and that it does not decay. Wong et al (1993) do not impose a large scale forced ascent, they find that in their simulation the squall line reaches the mature stage after 3 hours and decays slowly after that time. Another difference is that Tao et al (1993) use a cold pool to initialize the convection whereas Wong et al (1993) use a warm bubble with a small cooling rate upwind of the bubble. This difference is probably not very important.

Initially the same starting conditions as Tao et al (1993) were used. However the relative airflow through the simulated system was not very realistic and only a small stratiform region was produced, although the system was long lived. Using a wind profile similar to Wong et al (1993) improved the simulation considerably.

In other respects the initial conditions used by this simulation are similar to those used by Tao et al (1993). A large scale upward motion is imposed with a maximum vertical velocity of $7\,cms^{-1}$ at $1300\,m$. This upward motion decreases linearly with height to zero at $4400\,m$. Because of the periodic boundary conditions at the model's lateral boundaries a true large scale upward motion cannot be applied. Rather, the cooling and moistening effect of the large scale upward motion on the basic state is applied. A cold pool ($-5^o\,K$) is used to initiate the convection.

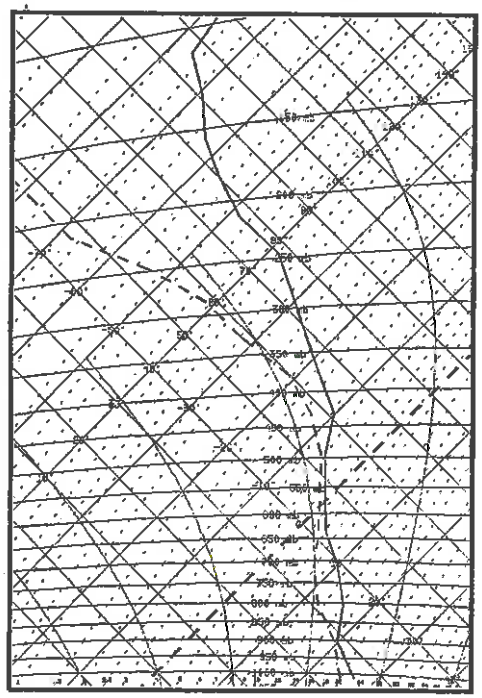

Figure 1: Initial model profile of temperature (solid line) and dew point (broken line).

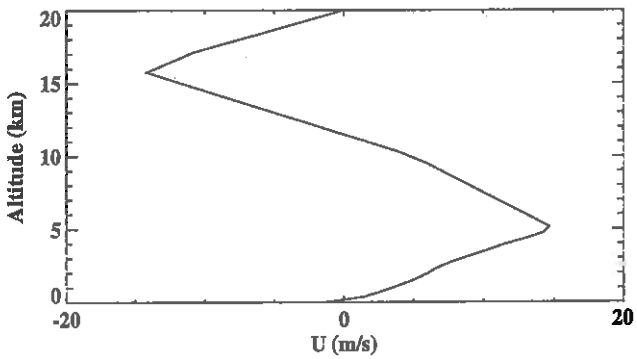

Figure 2: Initial model profile of horizontal wind along the direction of squall line propagation.

4.2 Model Results

The model produces a system with a vertical extent of about $15\,km$ and a wide trailing stratiform region, as shown in figure 3. This is in good agreement with observations and the simulation by Wong et al (1993). The expected radar reflectivity for the model precipitation is also calculated and is in good agreement with the observed radar reflectivity (figure 5). As would be expected most of the rain water is below the freezing level (about $5\,km$) and the largest rain water amounts are in the convective region. Graupel is found mainly between $5\,km$ and $10\,km$ in the convective region. The anvil is composed primarily of cloud ice and snow. The model squall line propagates with a speed of about $12\,ms^{-1}$ which compares well with speeds deduced from satellite observations.

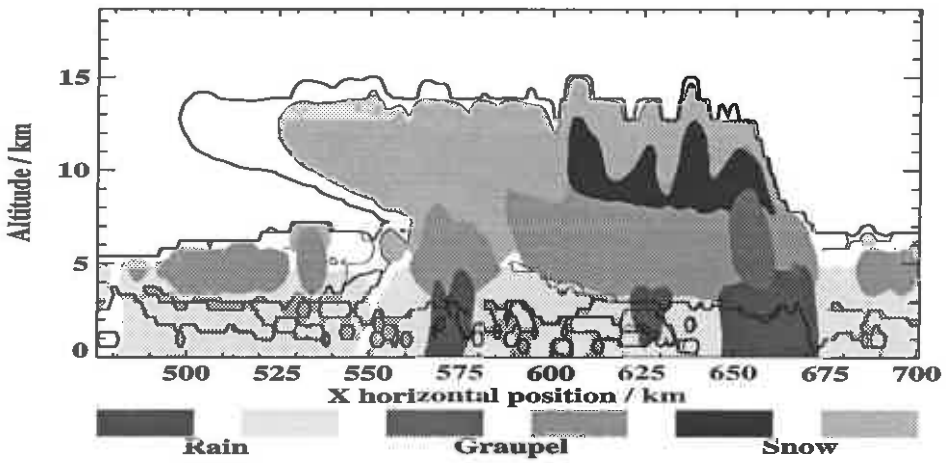

Figure 3: Model cloud and precipitation 7 hours into the simulation. The solid line encloses a region with the sum of cloud water, cloud ice, graupel and snow greater than $0.001\,g/kg$. The shaded regions show rain, graupel and snow as described by the key. Darker shaded regions show amounts greater than $0.5\,g/kg$ and lighter shaded regions show amounts greater than $0.01\,g/kg$. Note that only a part of the model domain is shown. The squall line is propagating to the right.

The vertical velocities predicted by the model are also in good agreement with those deduced from measurements of particle vertical velocities by the tail radar of the NOAA WD-P3 aircraft (see figure 5). Both model and observations show a maximum vertical velocity of about $10\,ms^{-1}$ located at a height of $10\,km$ and that the convective updraft

slopes rearward with height. The simulation by Tao et al (1993) also predicts a maximum updraft of about $10\,ms^{-1}$ but the simulation by Wong et al (1993) produces a maximum updraft of only $4\,ms^{-1}$.

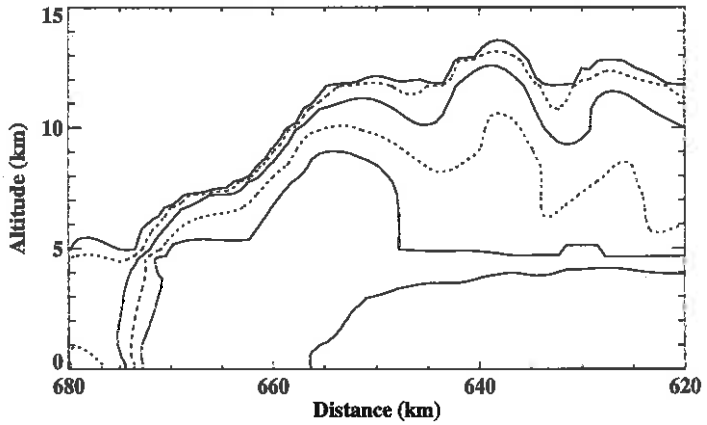

Figure 4: Calculated radar reflectivity (dBZ) for the model precipitation 7 hours into the simulation. Solid lines are at 5,23 and 41 dBZ and broken lines at 14 and 32 dBZ. The innermost solid line corresponds to 41 dBZ. To aid comparison with the observed radar reflectivity the horizontal axis has been reversed so that the squall line is propagating to the left.

Figure 7 shows the temperature at the lowest model level ($200\,m$). At the cold pool edge there is a sharp drop in temperature of about $3°C$. This is in good agreement with low level ($100\,m$) flight data from the CSIRO F27 aircraft (see figure 8). The F27 flew across a narrow arc shaped feature intersecting the main part of the squall line. This explains the much smaller size of the cold pool observed by the F27. The wind along the squall line propagation direction at the lowest model level is shown in figure 9. The gust front at the edge of the cold pool is clearly visible. Again this was also shown by the F27 data, although the details are different. The F27 measured a step like function for the velocity with small wind speeds ahead of the cold pool and a rapid increase in wind speed at the cold pool edge.

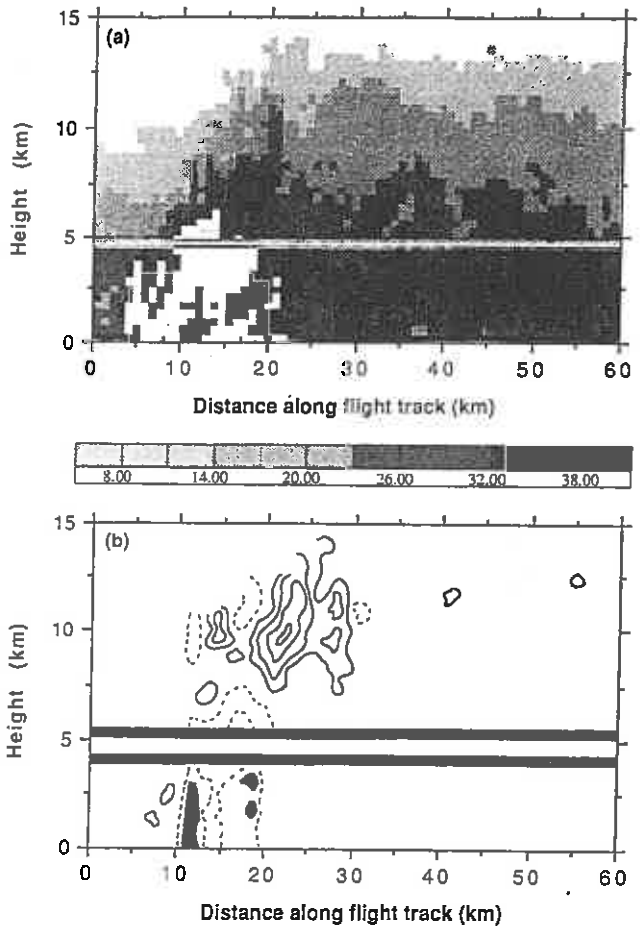

Figure 5: Time-height section of vertically pointing data from the P3 tail radar. Time is converted to horizontal distance under the assumption of a ground speed of $140\,ms^{-1}$. (a) Radar reflectivity and (b) Doppler vertical velocity of the precipitation particles. Solid lines show upward motion of 1,3,5 and $7\,ms^{-1}$. Dashed line shows downward motion of $-4\,ms^{-1}$ above the melting layer ($\simeq 5\,km$) and $-10\,ms^{-1}$ below, filled areas show vertical velocity $< -12\,ms^{-1}$. Air motions can be estimated by adding $1-2\,ms^{-1}$ to the radar detected velocities, above the melting layer, to account for the fall speed of snow particles. Below the melting layer, air motions can be estimated by adding $5-8\,ms^{-1}$ to account for the fall speed of rain drops. The flight level ($4.8\,km$) is evident in both panels. The Doppler range delay zone above and below the aircraft are contained within the heavy horizontal lines in (b). From Webster and Houze (1991).

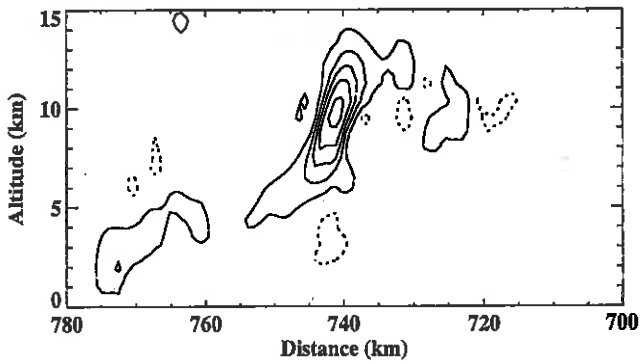

Figure 6: Vertical velocity predicted by the model 9 hours into the simulation. Solid lines show ascent with contour intervals of 1,3,5,7 and $9 ms^{-1}$. The broken line shows descent of $-1\, ms^{-1}$.

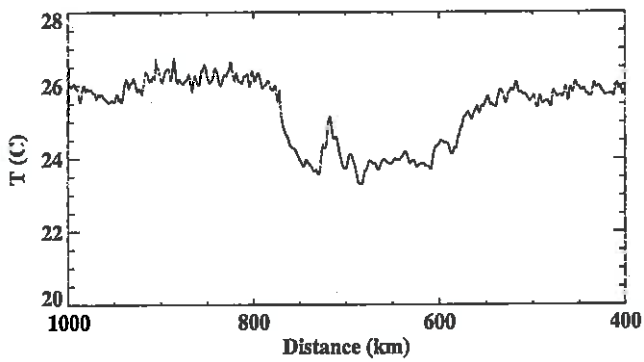

Figure 7: Temperature in lowest model level ($200\, m$) 9 hours into the simulation.

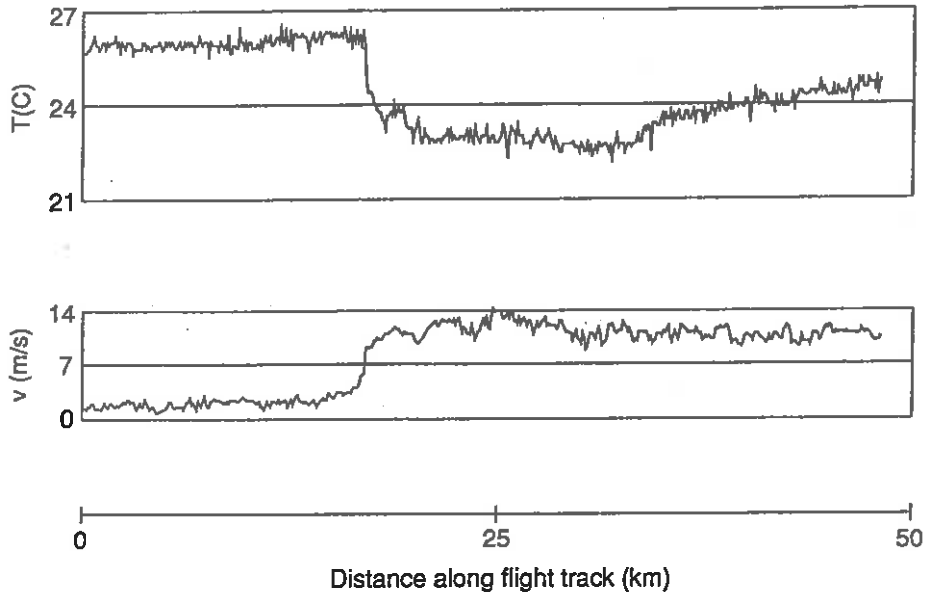

Figure 8: Time-series of temperature and wind parallel to the flight direction observed from the low level ($100\,m$) flight by the CSIRO F27 aircraft. From Webster and Houze (1991).

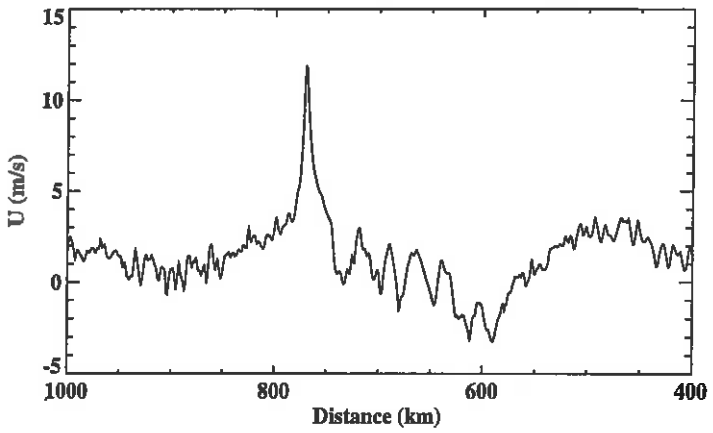

Figure 9: Velocity along the squall line propagation direction at the lowest model level ($200\,m$) 9 hours into the simulation.

4.3 Longwave Radiative Heating

The calculated longwave heating rates are shown in figure 10 and show substantial horizontal variation through the cloud. This is related to the variation of cloud water and cloud ice within the cloud. Maximum cooling rates are found at cloud tops and have magnitudes of upto $30\,K/day$ which is in good agreement with the results of Tao et al (1993) and Wong et al (1993). Cooling in the anvil extends over a substantial depth. This is because cloud ice amounts within the anvil are small so that absorption is relatively weak. If the anvil behaved as a black body then all the cooling would be localized at the surface (skin). Maximum cloud base warming rates are found to be around $10\,K/day$, while the clear air has an average cooling rate of about $2\,K/day$. Figure 11 shows a vertical profile of the domain wide horizontally averaged longwave radiative heating rate. The effect of cloud top cooling is readily apparent. Cloud base warming is masked by the presence of clear air cooling. Figure 12 shows the net longwave flux at the top of the atmosphere (TOA). The squall line reduces the outgoing TOA longwave flux by as much as $150\,Wm^{-2}$ and thus significantly reduces the longwave cooling.

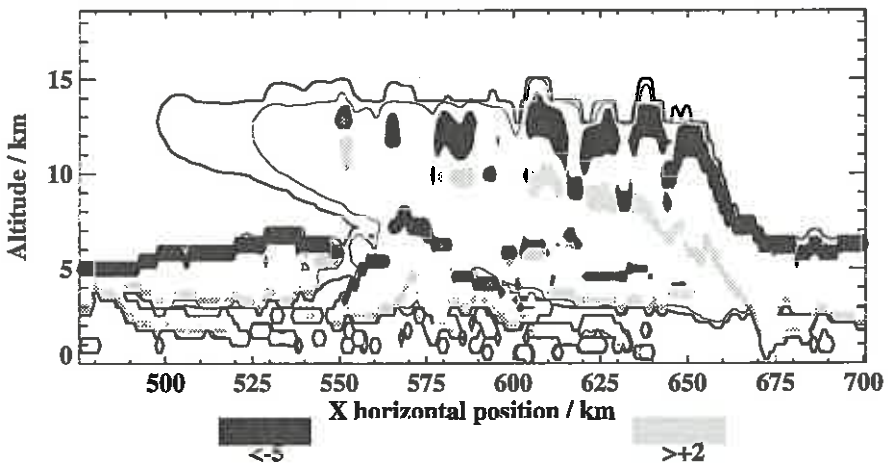

Figure 10: Calculated longwave radiative heating rates (Kelvin/day) 7 hours into the simulation.

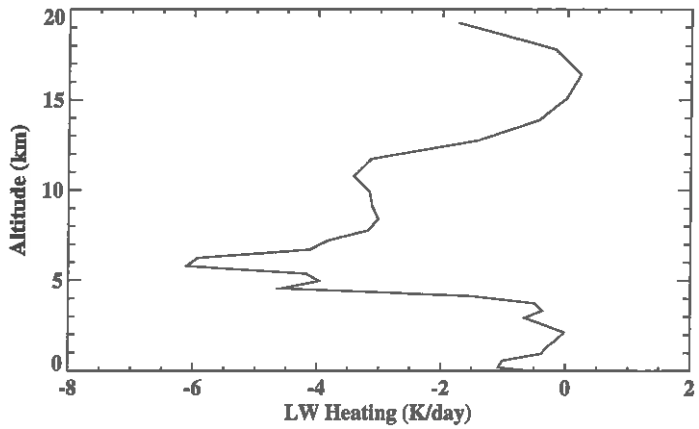

Figure 11: Calculated domain wide horizontally averaged longwave heating rate 7 hours into the simulation.

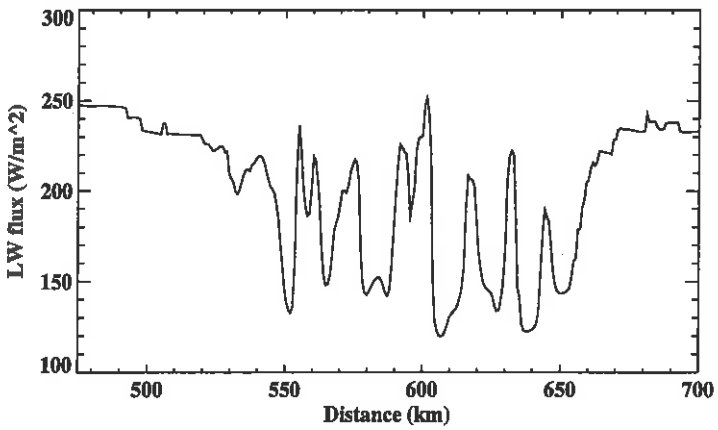

Figure 12: Calculated top of the atmosphere longwave flux 7 hours into the simulation.

5 Sensitivity To Longwave Radiative Heating

A simulation is run in which longwave radiative heating and cooling are removed. Rainfall rates for the two simulation are shown in figure 13. Removing longwave radiative heating reduces the total rainfall at 16 hours by 12 %. Tao et al (1993) find that removing longwave heating reduces total rainfall by 31 % for their simulations. Wong et al (1993) did not perform any sensitivity experiments.

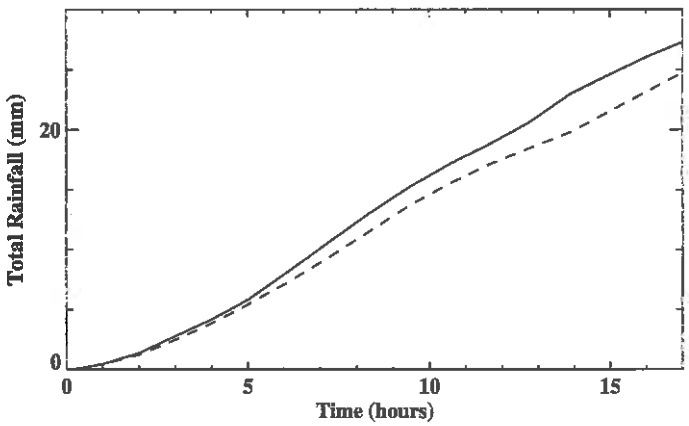

Figure 13: Domain wide horizontally averaged cumulative surface rainfall. The solid line is for the simulation including longwave radiative heating. The broken line is for the simulation with no longwave radiation.

Rainfall rates are shown in figure 14. The rainfall rates including longwave radiative heating are about 30 % greater than those given by Tao et al (1993). One possibility is that differences in initial conditions (perhaps due to differences in the vertical grid used) mean that there is less moisture inflow or cooling by the forced ascent in their model, which would explain the greater effect of longwave radiative heating in their model. Dudhia (1989) claims that convective activity is controlled to a large extent by the general cooling of the troposphere due to radiative processes and forced ascent. Thus smaller cooling by the forced ascent would increase the relative importance of radiative cooling. Another possibility is that the model used by Tao et al (1993) is less efficient at precipitating out the moisture inflow due to the forced ascent. Consequently the ability of longwave radiative heating to enhance rainfall would be greater in their model. The no longwave radiation simulation produces a smaller trailing stratiform region. Maximum vertical velocities are not significantly different between the two simulations, the largest vertical velocities are actually found in the no longwave radiation simulation. Squall line

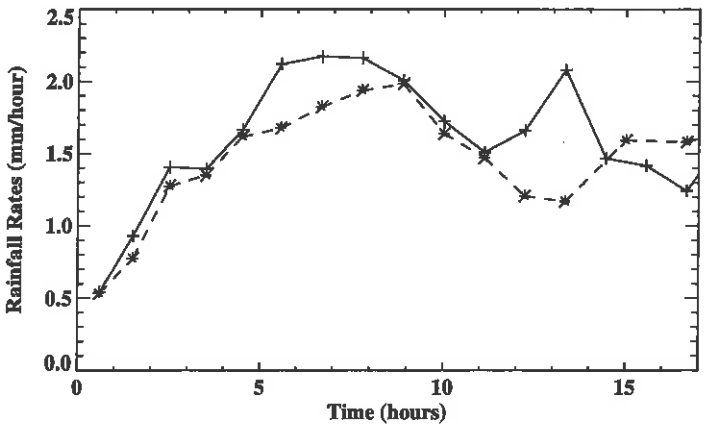

Figure 14: Domain wide horizontally averaged surface rainfall rates. The solid line is for the simulation including longwave radiative heating. The broken line is for the simulation with no longwave radiation.

propagation speeds are also similar in the two simulations. The potential temperature perturbation from the initial state is shown in figure 15 for the two simulations. As expected longwave radiation cools the troposphere and partially counters the warming due to the convective activity. Determination of the relative importance of the various radiative forcing mechanisms is left to a later study.

6 Discussion And Future Work

The two-dimensional version of the Meteorological Office cartesian large eddy simulation model is used to model a tropical squall line and successfully reproduce many of the features observed during EMEX9. Sensitivity studies show that the absence of longwave radiative heating reduces rainfall but that the magnitude of this reduction is not as large as that found by Tao et al (1993). This study is a first step in an effort to quantify the interaction of clouds and radiation and the effects of radiative heating on convective systems. Further studies are underway to improve understanding of the radiative forcing mechanisms and study the results of improvements to the radiation parametrization.

Future studies will determine the relative importance of the three radiative forcing mechanisms described in the introduction. This can be achieved by smoothing out spa-

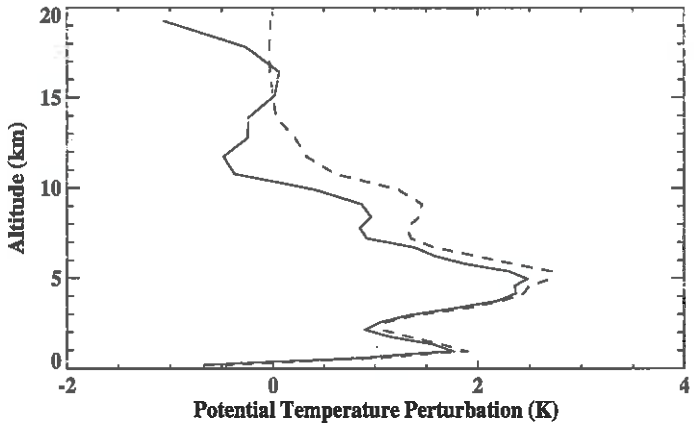

Figure 15: Vertical profile of the domain wide horizontally averaged potential temperature perturbation 7 hours into the simulation. The solid line is for the simulation including longwave radiative heating. The broken line is for the simulation with no longwave radiation.

tial variations in the longwave radiative heating. Removing all spatial variations will show whether it is only the large scale longwave radiative cooling which is important, as found by Dudhia (1989). By smoothing out horizontal variations it is possible to determine whether cloud/clear sky variations in radiative heating are important.

By smoothing in the vertical it may be possible to determine the importance of cloud top cooling and cloud base warming by longwave radiation. However, it may be that the vertical resolution of the model is too coarse for this effect to show. Miller and Frank (1993) find that cloud top cooling and cloud base warming has only a minor effect on precipitation in their model. Furthermore, the radiative heating rates calculated at cloud top and cloud base by their model are only half those given by Webster and Stephens (1980). The model used by Miller and Frank (1993) has a much coarser vertical resolution and this is the most likely cause for the difference. The importance of the model vertical resolution can be understood by the following argument. For clouds with high water contents, at cloud top the longwave radiative cooling is localized near the surface and decays rapidly into the bulk of the cloud. However the cooling rate calculated by the radiation scheme is an average for a model grid box. Thus this average includes the large cooling rates near the cloud top surface and the much smaller cooling rates in the bulk. Therefore the wider a model layer, the greater the contribution by the bulk to the average cooling rate, and hence a smaller calculated cooling rate. A similar argument applies to cloud base warming. Another effect will occur if a cloud occupies only a single model level. In this case both cloud top cooling and cloud base warming will occur in the same grid box

and partially cancel. Usually cloud top cooling has a greater magnitude than cloud base warming, thus the effect of the longwave radiation scheme will be to (incorrectly) cool the entire cloud. To determine the importance of radiative destabilization by cloud top cooling and cloud base warming it may be necessary to run cloud models with many more than the 20 to 30 levels currently used.

Dudhia (1989) states that convective activity is modulated by the cooling of the troposphere by longwave radiation and forced vertical motion. Following Cotton and Anthes (1989) the rate of precipitation reaching the surface P is related to the apparent heat source Q_1, radiative heating Q_R and the sensible heat flux H_s by

$$P = \frac{C_p}{Lg} \int_{p_t}^{p_s} (Q_1 - Q_R)\, dp - \frac{H_s}{L} \tag{2}$$

where

$$Q_1 = \frac{1}{C_p} \left[\frac{\partial \bar{s}}{\partial t} + \nabla.(\bar{\mathbf{V}}\bar{s}) + \frac{\partial \bar{\omega}\bar{s}}{\partial p} \right] \tag{3}$$

and $s = C_pT + gz$ is the dry static energy. If it is assumed that Q_1 is only slightly changed between the simulations including or excluding longwave radiation then the increase in rainfall due to longwave radiative cooling can be calculated from (2). Assuming that $Q_R = -2K/day$ and that the cloud top pressure p_t is $200\,mb$ and the surface pressure p_s is $1000\,mb$ predicts an increase in the rainfall rate of $0.27\,mm/hour$. This is an over estimate but considering the simplicity of the above argument the agreement with the model results is reasonable (see figure 14). Further experiments will be performed to determine the usefulness of the above approximation and to understand the relative importance of longwave radiation to forced vertical motion.

As described in section 3, the most important weakness of the longwave radiation scheme is the treatment of absorption by cloud ice. The value of κ_{Ice} used in the longwave radiation scheme is equivalent to assuming that the ice crystal effective radius is always $20\,\mu m$. However the actual ice crystal effective radius will depend on quantities such as temperature and ice water content. A possible way to improve the longwave radiation scheme is to use the ice microphysics to determine the ice crystal effective radius. However, the ice microphysics parameters are tuned to give accurate conversion rates and may not give reliable values for other quantities. Alternatively empirical data could be used to parameterize the ice crystal effective radius, for example Sun and Shine (1993). Possible problems with this approach include the limited amount of experimental data available and that much of the data collected is for mid-lattitude cirrus. Such data may not be representative for the anvils of tropical storms.

The longwave radiation scheme ignores the effect of rain, snow and graupel. However

snow is an important constituent of the anvil (figure 3) and this may be a significant omission. The rationale for ignoring absorption by the precipitation particles is that they are much larger than cloud droplets or cloud ice crystals. Therefore for a given amount, precipitation particles have a smaller total cross-sectional area than cloud droplets or cloud ice crystals. Consequently, precipitation particles do not absorb as strongly. However, precipitation particles are likely to absorb more strongly than clear air.

A possible method for including the effect of snow and graupel is to treat absorption by these in the same way as absorption by cloud ice. However, the assumption that the ice particle effective radius is $20\,\mu m$ is even worse for snow and graupel than it is for cloud ice crystals. The ice microphysics assumes an inverse exponential distribution for the size spectra of snow and graupel and this could be used to calculate the effective radius. Dharssi (1994) describes such an approach to calculate the effective radius of rain and a simple parametrization of the effect of rain on longwave radiation.

The simulations described in this article do not include shortwave radiative heating. The simulation by Tao et al (1993) does not include shortwave radiative heating either. Wong et al (1993) include shortwave radiative heating and find maximum heating rates of $33\,K/day$ at cloud tops. Therefore, shortwave radiative heating is likely to have an important effect on convective systems and will need to be included in future studies.

7 References

Cotton W. and Anthes R. 1989. Storms and Clouds. International geophysics series, volume 44. Academic press.

Derbyshire S. and Kershaw R. 1993. Turbulence simulation in the Met. Office. *Met. Mag*, **122**, 25-34.

Dharssi I. 1994. The effect of rain on longwave radiation. *Internal Report*, No. **9**, JCMM.

Dudhia J. 1989. Numerical study of convection observed during the Winter Monsoon Experiment using a mesoscale two-dimensional model. *J. Atmos. Sci.* , **36**, 586-601.

Francis P., Jones A., Saunders R., Shine K., Slingo A. and Sun Z. 1994. *Submitted to Q.J.R. Met. Soc.*

Gray W. and Jacobson R. 1977. Diurnal variation of oceanic deep cumulus convection. *Mon. Wea. Rev.*, **105**, 1171-1188.

Ingrams W. 1993. Radiation. Unified model documentation paper 23. United Kingdom Meteorological Office.

Lin Y., Farley R. and Orville H. 1983. Bulk parametrization of the snow field in a cloud model. JCAM, **22**, 1065-1092.

Miller R. and Frank W. 1993. Radiative forcing of simulated tropical cloud clusters. *Mon. Wea. Rev.*, **121**, 482-498.

Slingo A. and Wilderspin R. 1986. Development of a revised longwave radiation scheme for an atmospheric general circulation model. *Q.J.R. Met. Soc.*, **112**, 371-386.

Stephens G. 1984. The parametrization of radiation for numerical weather prediction and climate models. *Mon. Wea. Rev.*, **112**, 826-867.

Sun Z. and Shine K. 1993. Studies of radiative properties of ice and mixed phase clouds. *Submitted to Q.J.R. Met. Soc.*

Swann H. 1994. Cloud microphysical processes - a description of the parametrization used in the Large Eddy Model. *Internal Report*, No. **10**, JCMM.

Tao W., Simpson J., Sui C., Ferrier B., Lang S., Scala J., Chou M. and Pickering K. 1993. Heating, moisture and water budgets of tropical and midlatitude squall lines: comparison and sensitivity to longwave radiation. *J. Atmos. Sci.*, **50**, 673-890.

Webster P. and Houze R. 1991. The equatorial mesoscale experiment (EMEX): An overview, *Bull. Amer. Meteor. Soc.*, **72**, 1481-1505.

Webster P. and Stephens G. 1980. Tropical upper-tropospheric extended clouds: Inferences from winter MONEX. *J. Atmos. Sci.*, **37**, 1521-1541.

Wong T., Stephens G. and Stackhouse W. 1993. The radiative budgets of a tropical mesoscale convective system during the EMEX-STEP-AMEX experiment. Part 2, Model results. *J. Geophys. Res.*, **98**, *no* D5, 8695-8711.

33. **Observations of the mesoscale sub-structure in the cold air of a developing frontal cyclone**
K A Browning, S A Clough, C S A Davitt, N M Roberts and T D Hewson
May 1994

34. **Longwave Radiative Forcing of a Simulated Tropical Squall Line**
Imtiaz Dharssi
July 1994

CURRENT JCMM INTERNAL REPORTS

This series of JCMM Internal Reports, initiated in 1993, contains unpublished reports and also versions of articles submitted for publication. The complete set of Internal Reports is available from the National Meteorology Library on loan, if required.

1. **Research Strategy and Programme.**
   K A Browning et al
   January 1993

2. **The GEWEX Cloud System Study (GCSS).**
   GEWEX Cloud System Science Team
   January 1993

3. **Evolution of a mesoscale upper tropospheric vorticity maximum and comma cloud from a cloud-free two-dimensional potential vorticity anomaly.**
   K A Browning
   January 1993

4. **The Global Energy and Water Cycle**
   K A Browning
   July 1993

5. **Structure of a midlatitude cyclone before occlusion.**
   K A Browning and N Roberts
   July 1993

6. **Developments in Systems and Tools for Weather Forecasting.**
   K A Browning and G Szejwach
   July 1993

7. **Diagnostic study of a narrow cold frontal rainband and severe winds associated with a stratospheric intrusion.**
   K A Browning and R Reynolds
   August 1993

8. **Survey of perceived priority issues in the parametrizations of cloud-related processes in GCMs.**
   K A Browning
   September 1993

9. **The Effect of Rain on Longwave Radiation.**
   I Dharssi
   September 1993

10. **Cloud Microphysical Processes - A Description of the Parametrization used in the Large Eddy Model.**
H Swann
July 1994

11. **An Appreciation of the Meteorological Research of Ernst Kleinschmidt.**
A J Thorpe
May 1992

12. **Potential Vorticity of Flow Along the Alps.**
A J Thorpe, H Volkert and Dietrich Heimann
August 1992

13. **The Representation of Fronts.**
A J Thorpe
January 1993

14. **A Parametrization Scheme for Symmetric Instability: Tests for an Idealised Flow.**
C S Chan and A J Thorpe
February 1993

15. **The Fronts 92 Experiment: a Quicklook Atlas.**
Edited by T D Hewson
November 1993

16. **Frontal wave stability during moist deformation frontogenesis. Part 1. Linear wave dynamics**
C H Bishop and A J Thorpe
May 1993

17. **Frontal wave stability during moist deformation frontogenesis. Part 2. The suppression of non-linear wave development.**
C H Bishop and A J Thorpe
May 1993

18. **Gravity waves in sheared ducts.**
S Monserrat and A J Thorpe
October 1993

19. **Potential Vorticity and the Electrostatics Analogy: Quasi-Geostrophic Theory.**
C Bishop and A J Thorpe
November 1993

20. **Recent Advances in the Measurement of Precipitation by Radar.**
A J Illingworth
April 1993

21. **Micro-Physique et Givrage. Cloud Microphysics and Aircraft Icing.**
A J Illingworth
May 1993

22. **Differential Phase Measurements of Precipitation.**
M Blackman and A J Illingworth
May 1993

23. **Estimation of Effective Radius of Cloud Particles from the Radar Reflectivity.**
N I Fox and A J Illingworth
May 1993

24. **A Simple Method of Dopplerising a Pulsed Magnetron Radar.**
L Hua, A J Illingworth and J Eastment
November 1993

25. **Radiation and Polar Lows.**
George C Craig
February 1994

26. **Collected preprints submitted to International Symposium on the Life Cycles of Extratropical Cyclones; Bergen, Norway, 27 June - 1 July 1994**
April 1994

27. **Convective Frontogenesis**
Douglas J Parker and Alan J Thorpe
April 1994

28. **Improved Measurement Of The Ice Water Content In Cirrus Using A Total Water Evaporator**
Philip R A Brown and Peter N Francis
April 1994

29. **Mesoscale Effects of a Dry Intrusion within a Vigorous Cyclone**
K A Browning and B W Golding
April 1994

30. **GEWEX Cloud System Study, Science Plan**
May 1994

31. **Parametrization of Momentum Transport by Convectively Generated Gravity Waves**
R Kershaw
May 1994

32. **Mesoscale Modelling Newsletter, No. 5**
May 1994

Met Office Joint Centre for Mesoscale Meteorology Department of Meteorology
University of Reading PO Box 243 Reading RG6 6BB United Kingdom
Tel: +44 (0)118 931 8425 Fax: +44 (0)118 931 8791
www.metoffice.com